Chapter 2

Experimental Procedures and Introduction to Techniques

This chapter presents an introduction to electrode/solution interfaces. This includes a brief discussion of the composition of the electrode/solution interface including an explanation into the double layer and the associated capacitance. Electron transfer is discussed with attention given to both homogeneous and heterogeneous electron transfer, the latter of which is applicable to electron transfer at an electrode/solution interface. The main electrochemical techniques used throughout this thesis are cyclic voltammetry and differential pulse voltammetry, both of which are discussed in section 2.1.5. The electronic properties of transition metal complexes along with an introduction to Raman spectroscopy are detailed in section 2.2 and 2.3 respectively. The experimental conditions used for each technique described throughout this thesis are given in section 2.4.

2.1 Electrochemistry

2.1.1 Introduction

Since the early days of the 19th century when Volta first discovered the Voltaic pile (or the first battery) electrochemistry has become a phenomenon that is widely used in a variety of disciplines throughout science.[1] From biology and chemistry, to physics and materials science you will uncover interfaces, a lot of which carry a charge. Electrochemistry becomes a very valuable tool when trying to understand and determine how such charges interact, e.g. chemical reactions and electron transfer at electrode – solution interfaces.

Contributions to the principles behind electrochemical phenomena from influential scientists such as Michael Faraday and others saw the area of electrochemistry grow throughout the 19th and early 20th centuries - even before Thompson discovered the electron in 1923. From the early uses of potentiometry and polarography and throughout the late 20th century, significant advances in electrochemical theory and methods have made this an increasingly important tool in the study of chemical systems.

Chapters 3 to 6 in this thesis focus on the diffusion controlled (and surface confined in Chapters 3 and 5) electrochemical properties of a range of transition metal complexes with an organic tetrathiafulvalene derivative being the topic of discussion in Chapter 5. Cyclic voltammetry and differential pulse voltammetry are the main electrochemical techniques employed where the potential is varied as a function of time and a current response is obtained. A general introduction into the principles behind both of these techniques is given in this chapter.

2.1.2 Electrode/Solution Interface and the Double Layer

In an electrochemical cell there are two different types of processes that can occur at an electrode. The first of these is the charge transfer reaction where the passage of charge, in the form of electrons, occurs between the electrode/solution interface. Faraday's first law states that the quantity of a chemical species, produced by

electrolysis, is proportional to the amount of electrical current used.[1] As these charge transfer reactions occurring at the metal/solution interface are governed by this law, they are labelled as Faradaic processes. Potential regions exist where no Faradaic processes or charge transfer reactions occur because they are considered thermodynamically or kinetically unfavourable at such potentials. Even though no charge passes within the electrode/solution interface, other processes can take place including adsorption and desorption. The structure of the electrode/solution interface can change with changes in potential and consequently the solution composition may alter. Events such as these can lead to the flow of an external current even though no electrons cross the interface. Such processes are known as nonfaradaic processes.[2] Electrode reactions involving chemical species result in not only Faradaic, but also nonfaradaic processes taking place. To fully understand chemical reactions at electrode/solution interfaces the effects of both of these processes must be considered.

Charge transfer reactions occurring at the electrode/solution interface are in a different environment to that of the homogeneous bulk solution. In the latter, the species is in an isotropic environment and there is an absence of an electric field. However, the electric field at the electrode/solution interface is anisotropic as a result of a breakdown of symmetry. The effect of this anisotropic electric field on the species is dependent on distance and decreases with increasing distance from the electrode surface.[3]

Polarization of solvent dipoles leads to their orientation at the solution side of the interface and as a consequence a net ionic charge builds up. The electrode then responds by attracting a layer of ions to its surface, the charge of which is of equal quantity and opposite sign (positive electrodes draw negative ions and *vice versa*). This resulting charge separation produced by the local ordering of the ions at the electrode/solution interface is known as the electrical *double layer*.

Charge separation at interfaces was first considered in the mid 19th century when Helmholtz [4] proposed that the structure of the interface between a metal and a solution was like that of a parallel-plate capacitor, i.e. a device made up of two metal sheets which are separated by a dielectric material that is capable of storing charge. However, this was a somewhat naïve description as it is unlikely that the array of

charges on the solution side of the interface lie on a single plane because of thermal agitation resulting in the layer of charge diffusing into the bulk solution. This idea of a diffuse layer of charge on the solution side of the interface was introduced by Gouy [5] and Chapman [6] which describes how the concentration of excess charge is the greatest adjacent to the electrode as this is the point where the strength of the electrostatic forces are great enough to overcome the thermal processes. As the distance from this point toward the bulk solution increases, the concentration of charge gradually decreases. Limitations also exist in the Gouy-Chapman model. The proposal that the ions are considered as point charges that can approach the surface at any random point is unrealistic. Ions have a defined radius and tend to be solvated in approaching the metal surface. As a result of this, and the presence of solvent molecules at the metal/solution interface, their distance of closest approach will be greater than zero. This distance is dependent on the ionic radius, the solvation shell around the ion and the electrostatic interaction. This is taken into consideration in the Stern approach [7] to the structure of the double layer.

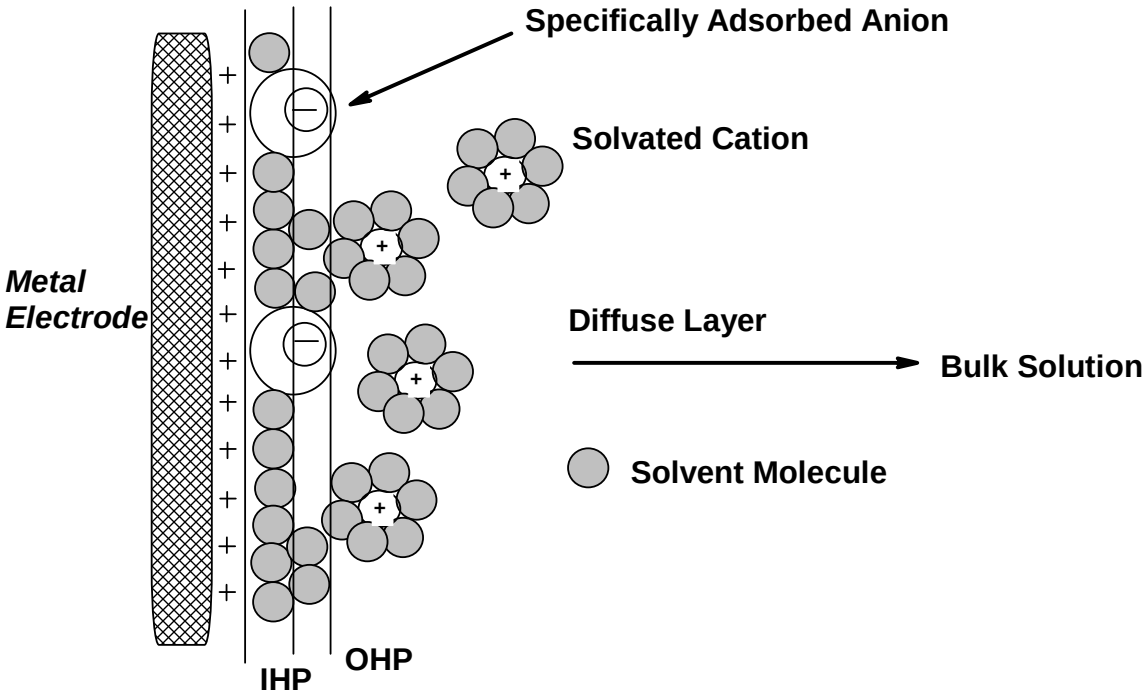

Figure 2.1: *Proposed structure of the double layer region including the inner and outer Helmholtz planes as proposed by the Stern model.[7] Adapted from reference 2.*

The interface itself is considered to consist of a layer of atoms (ions) on the surface with a single layer of adsorbed solvent molecules and other specifically adsorbed ions. The actual double layer itself is comprised of several layers, including this inner layer of specifically adsorbed ions, which extends to the bulk solution trailing off as a result of Brownian motion.[8] The inner layer of this interfacial region (not to be confused with the bulk phase) that houses the specifically adsorbed ions (including anions) is known as the *inner Helmholtz plane* (IHP), Figure 2.1. Anions, capable of shedding their solvation sphere, bind strongly to the metal surface and are therefore also considered to be part of the IHP.

Non-specifically adsorbed species in the diffuse layer of the interfacial region include solvated cations and also, in the case of modified electrodes, monolayer or polymer films.[3] Cations are more easily solvated as a result of their small radii leading to high free energies of solvation. The solvated cations are less likely to loose their solvation sheath even if the electrode is negatively charged: the distance of closest approach will therefore depend on the radius of the inner solvent-coordination sphere. The outer diffuse layer (which extends from the inner layer out to the bulk solution) comprised of these solvated cations is known as the *outer Helmholtz plane* (OHP). Finally, a *potential of zero charge* (PZC) also exists where, in the absence of specific adsorption, no net charge exists as a result of an equal number of cations and anions in the OHP.

2.1.3 Differential Capacitance

Capacitors are devices used in electrical circuits capable of storing electric charge. If the double layer is considered to behave like a parallel plate capacitor then its capacitance, C_{dl} is proportional to the stored charge of the layer and is a function of the potential applied to the metal/solution interface. Changes to the potential applied across the interface will alter the capacitance of the double layer. In real electrochemical systems the double layer does not behave like a parallel-plate capacitor. Perturbation of the applied potential across the double layer alters the orientation of the solvent dipoles and leads to adsorption and desorption of ions as well as the consequent change in the charge stored. The capacitance of the double layer is more appropriately referred to as the differential capacitance, C_d: the change

in the stored charge within the double layer is induced by changes in the applied potential and is a function of the potential.[9]

Although the charge stored at the interface changes as a function of the applied potential across the double layer, there is generally a potential region whereby the C_d remains approximately constant.[8] This double layer capacitance is usually in the range of 10 – 40 μF cm^{-2} [2], the minimum of which is found at the PZC.[3]

Where the surface of the electrode is unmodified, the differential capacitance is considered to be comprised of two contributing components: on the solution side of the double layer, the capacitance of the OHP, C_{OHP} as well as the capacitance of the diffuse layer, C_{diff} add to the overall capacitance of the double layer. For capacitors in an electrical circuit, that are arranged in series, the total capacitance is found from the sum of the reciprocal of the capacitance of each capacitor in the series. The same logic can be applied when calculating the C_d of an unmodified surface, Equation 2.1.

Equation 2.1 $$1/C_d = 1/C_{OHP} + 1/C_{diff}$$

Modifying the electrode surface with a molecular layer significantly alters the capacitance of the Helmholtz layer. This region of the double layer that was made up of ions and solvent with a high dielectric constant now has a lower capacitance as a result of the reduced dielectric constant of the ion-free film – especially in the case of organic films like alkane-thiol monolayers.[3] The capacitance of the modified metal/solution interface is practically independent of the applied potential. Like that of the unmodified surface, the differential capacitance of the interface is calculated using the sum of the reciprocal of both the capacitance of the film, C_{film} and C_{diff}, Equation 2.2.

Equation 2.2 $$1/C_d = 1/C_{film} + 1/C_{diff}$$

As the modification of the electrode surface with a film prevents the specific adsorption of electrolyte ions, it is only the capacitance of the diffuse layer that is

deemed to depend on the applied potential or the ionic strength of the electrolyte solution. At high concentrations of ions the capacitance of the diffuse layer will be large and given the reciprocal nature of Equation 2.2 the differential capacitance will be dominated by the capacitance of the insulating molecular film. Chidsey *et al.* [10] reported that Au electrodes coated in an organic alkane thiol monolayer were used to demonstrate that longer chain alkane thiol monolayers show a linear relationship between the reciprocal of C_d and the numbers of $-CH_2$ groups. For dense monolayers that are defect free the limiting capacitance can be as low as 5 – 10 μF / cm^2.[2]

Interfacial supramolecular assemblies consisting of monolayers where the surface coverage is incomplete have areas of the electrode surface exposed to ions and solvent molecules from the electrolyte. Therefore the differential capacitance of the double layer in this instance can be considered as a series of capacitances in parallel. Using chronoamperometry Forster and Faulkner [11] observed that the double layer capacitance of an electrode modified with an osmium polypyridyl complex was half that of the unmodified electrode under the same electrolyte conditions. However, changing the redox composition of the monolayer through oxidation of the metal centre within the layer leads to an increase in the differential capacitance of the double layer. Oxidation may lead to charge compensating ions and solvent molecules from the electrolyte entering the monolayer and therefore increasing the dielectric constant or decreasing the distance of closest approach which may lead to an increase in the measured capacitance.

The formation of a monolayer requires the displacement of specifically adsorbed ions and solvent molecules from the interface. Therefore the capacitance of the double layer changes from that of the unmodified surface. Electrochemical techniques such as cyclic voltammetry, chronoamperometry and AC impedance spectroscopy can be used to determine the differential capacitance of the double layer at metal/solution interfaces.

2.1.4 Electron Transfer

Chemical reactions proceeding via electron transfer are considered to involve a radiationless electronic rearrangement of the reactant species involved. The reactants

and products can be molecular species or in the case of heterogeneous electron transfer can involve an electrode as the donor or acceptor of the electron involved in the reaction. Both homogeneous and heterogeneous electron transfer reactions are broadly explained in the Marcus theory.[12] This theory originally encompassed only outer sphere electron transfer reactions where the donor and acceptor species are independent of each other. However, since then it has been further developed to include inner sphere reactions where the reactants are chemically bonded and electron transfer is mediated using a molecular bridge. For the purpose of the following discussion on electron transfer the donor and acceptor system is represented by D-B-A. The component B is a connector between the reactive species and may represent a bridging unit for mediating electron transfer or a through space interaction. D and A, represent the reactant and product species and are photo- or redox active units. The components may also represent an electrode surface as in the case of heterogeneous electron transfer reactions.

2.1.4.1 Homogeneous Electron Transfer and the Marcus Theory

Homogeneous electron transfer describes electron transfer in chemical reactions where the driving force does not come from an external source and instead is dictated by the electronic nature of the reactants involved. The Marcus theory described the reaction coordinates of a homogeneous electron transfer reaction (Equation 2.3) as behaving as simple harmonic oscillators. Figure 2.2 illustrates the free energies of the reactant state D-B-A prior to electron transfer and the corresponding product state $D^{\bullet+}$-B-$A^{\bullet-}$ as a function of the associated reaction coordinates.

Equation 2.3 $\quad D\text{-}B\text{-}A \rightarrow D^{\bullet+}\text{-}B\text{-}A^{\bullet-}$

The Marcus microscopic model of electron transfer can be applied under two conditions. The first of these is that the energy within the system must be conserved according to the First Law of Thermodynamics.[3] Electron transfer reactions are considered to be radiationless processes where the transfer of an electron is an isoenergetic process; both the donor reactant state and the acceptor product state are of the same energy.

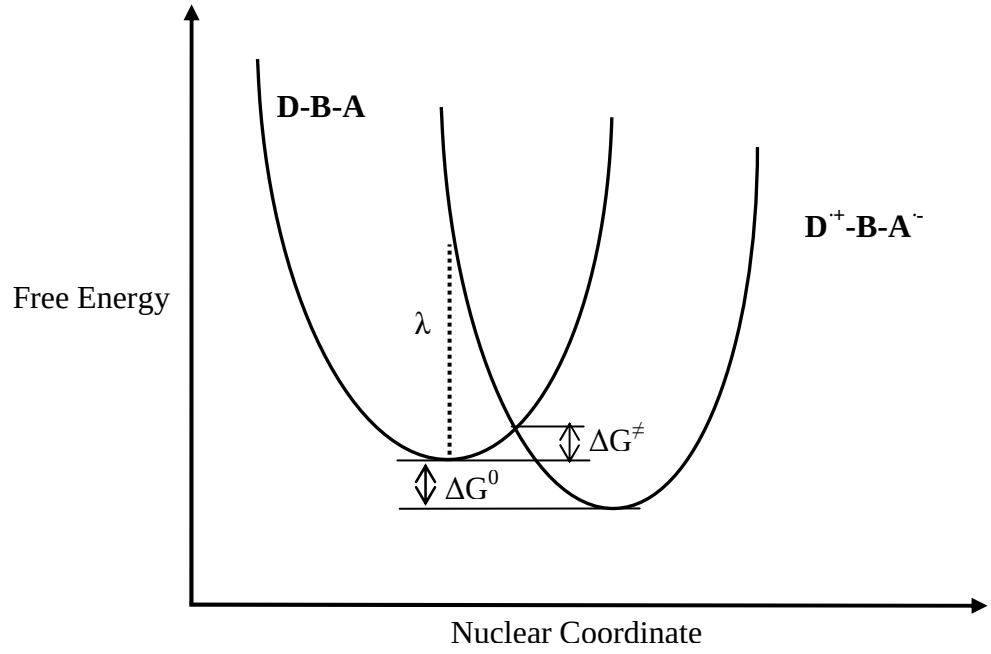

Figure 2.2: *Potential energy curves for the reactant and product states before and after a diabatic electron transfer reaction. Adapted from reference 3.*

The second requirement is that at the instant of electron transfer the reactant and product states are of the same nuclear geometry as stated under the Franck-Condon principle; electron transfer is an instantaneous process where no changes, either inner sphere or outer sphere, occur. At the crossing point of both curves in Figure 2.2 both of these conditions for electron transfer are fulfilled.

Equation 2.4 expresses the rate constant for the electron transfer process described in Equation 2.3, under the conditions of the First Law of Thermodynamics and the Franck Condon principle.

Equation 2.4 $$k = \nu_N \kappa \exp(-\Delta G^{\neq} / RT)$$

$$\Delta G^{\neq} = (\lambda/4)(1 + \Delta G^0/ \lambda)^2$$

where ν_N and κ represent the average nuclear frequency factor (S^{-1}) and electronic transmission coefficient respectively, λ is the reorganizational energy, $\Delta G^{\neq}$ is the free activation energy and ΔG^0 is the standard free energy of the reaction.[13]

2.1.4.2 The Reorganizational Energy λ and Gibbs Free Energy of Activation

The reorganizational energy, λ is the energy required to alter the nuclear geometries of the reactant state, and the solvent in the surrounding media, to that of the equilibrium geometry of the product state. There are two individual contributions to λ, Equation 2.5. The first of these is the inner sphere contribution, λ_i which arises from changes in the molecular geometry (bond lengths and angles) of the reactant when transforming to the product state. The outer sphere contribution, λ_o therefore reflects the distortion to the solvent and the reorientation of the surrounding media during the transition.

Equation 2.5 $\lambda = \lambda_i + \lambda_o$

For heterogeneous electron transfer processes involving a reactant species and an electrode, the major contribution to the λ is considered to come from the λ_o contribution as interfacial assemblies experience little changes in the bond lengths and angles during electron transfer processes such as oxidation or reduction at the electrode surface.[3] Equation 2.6 gives an expression for the outer sphere contribution to λ required to change the nuclear geometry of the reactant to that of the transition state configuration in a homogeneous electron transfer reaction.

Equation 2.6 $\lambda_o = e^2/(4\pi\varepsilon_0)\,(2r_D^{-1} + 2r_A^{-1} - d_{DA}^{-1})\,(\varepsilon_{op}^{-1} - \varepsilon_s^{-1})$

where *e* represents the electronic charge, r_D and r_A are the radii of the donor and acceptor species respectively, d_{DA} is the internuclear distance between the donor and acceptor molecules and ε_{op} and ε_s are the optical and static dielectric constants of the solvent in the surrounding medium. As λ_o is dependent on the dielectric constants of the surrounding medium, any changes in polarity of the solvent, or the distance between reactants will lead to a corresponding change in λ_o.

Equation 2.7 $\lambda_o = e^2/(8\pi\varepsilon_0)\,(r_X^{-1} - R^{-1})\,(\varepsilon_{op}^{-1} - \varepsilon_s^{-1})$

For a heterogeneous electron transfer reaction involving a molecular species with an electrode the λ_o may be expressed as in Equation 2.7 above, where r_X is the radius of

the reactant and R is twice the distance from the centre of the molecule to the electrode.[2]

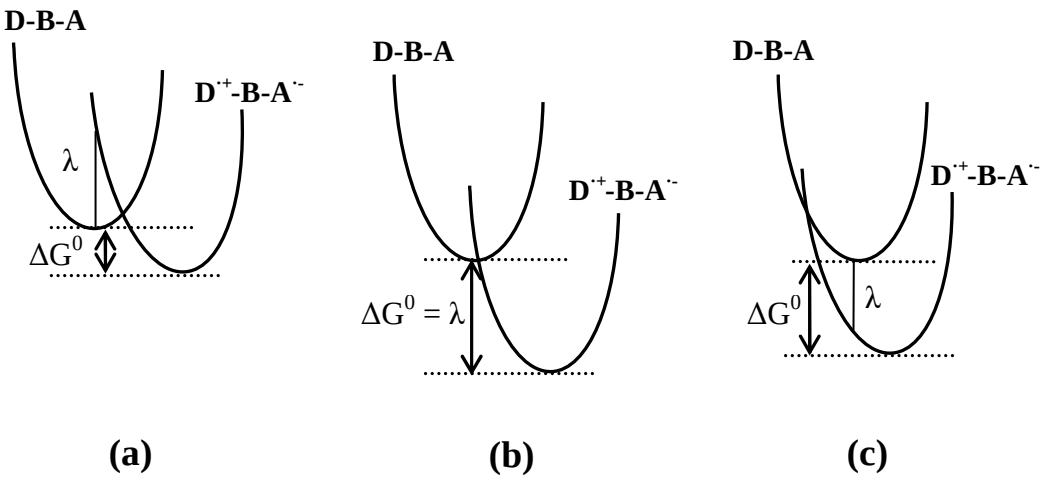

Figure 2.3: *Illustration of the reaction coordinate parabolic curves for diabatic electron transfer. (a) depicts the 'normal' region, where $\Delta G^0 < \lambda$, (b) represents the 'activationless' region, where $\Delta G^0 = \lambda$ and finally, (c) indicates the 'inverted' electron transfer region, where $\Delta G^0 > \lambda$. Adapted from reference 3.*

Equation 2.4 relates the electron transfer rate constant with the free energy of activation, $\Delta G^{\neq}$. It also demonstrates how $\Delta G^{\neq}$ varies with the thermodynamic driving force (overall free energy of electron transfer), ΔG^0 and λ. Three scenarios arise where changes in ΔG^0, at constant values for λ affect the $\Delta G^{\neq}$, Figure 2.3. In the *normal* region $\Delta G^{\neq}$ is predicted to decrease, as ΔG^0 increases (becomes more negative) and hence the rate constant, *k* increases. Where the transition state is found at the point of minimum energy of the nuclear coordinate of the reactant state ($\Delta G^{\neq} = 0$) λ has a value which equals ΔG^0 and the electron transfer is described as *activationless*. At this point the rate constant is thought to be at a maximum. Finally, where the activation energy increases in strongly driven reactions, ΔG^0 is less than $\Delta G^{\neq}$ and the rate of electron transfer decreases. This is known as the *inverted* region.

2.1.4.3 Diabatic and Adiabatic Electron Transfer

Electron transfer processes may be described as diabatic (also known as non-adiabatic) or adiabatic in nature. Before discussing these cases one must consider the frequency factor, ν which is a product of ν_N, the average nuclear frequency factor and κ, which is the electronic transmission coefficient. ν_N relates to the attempts of the

transferring electron to crossing the energy barrier and being promoted to the product state and κ is associated with electron tunnelling from reactant to product via the transition state.

Equation 2.8 $\nu = \nu_N \kappa$

The magnitude of κ reflects the degree of electronic coupling between the wavefunctions of the donor and acceptor species which is expected to decrease exponentially with increasing donor-acceptor distance. When the coupling is strong the crossing point of the potential energy curves of the reactant and product states is broadened, Figure 2.4 (bottom).

Equation 2.9 $k = \nu_N \exp(-\Delta G^{\neq} / RT)$

In this situation, κ is close to unity, i.e. there is a high probability of electron transfer from reactant to product occurring across a single energy surface. The flatter energy surface of the crossing point near the transition state leads to reduced rates of electron transfer. This type of electron transfer is known as an adiabatic process and the maximum rate is determined by ν_N according to Equation 2.9.

The second case of electron transfer processes is known as non-adiabatic electron transfer. The interaction between the reactant and product states is small and the electronic coupling is considered weak with a low probability of crossover between the two states. $\kappa << 1$ for this type of electron transfer and the crossover point of the two parabolic curves is sharp as opposed to the flattened surface observed for adiabatic processes. In order for the transferring electron to reach the product state it must pass through the transition state to a new energy surface, Figure 2.4. Non-adiabatic electron transfer is normally expected where the electronic coupling is weak. This arises when the donor and acceptor units are separated over a certain distance leading to long range coupling between the two components.[3]

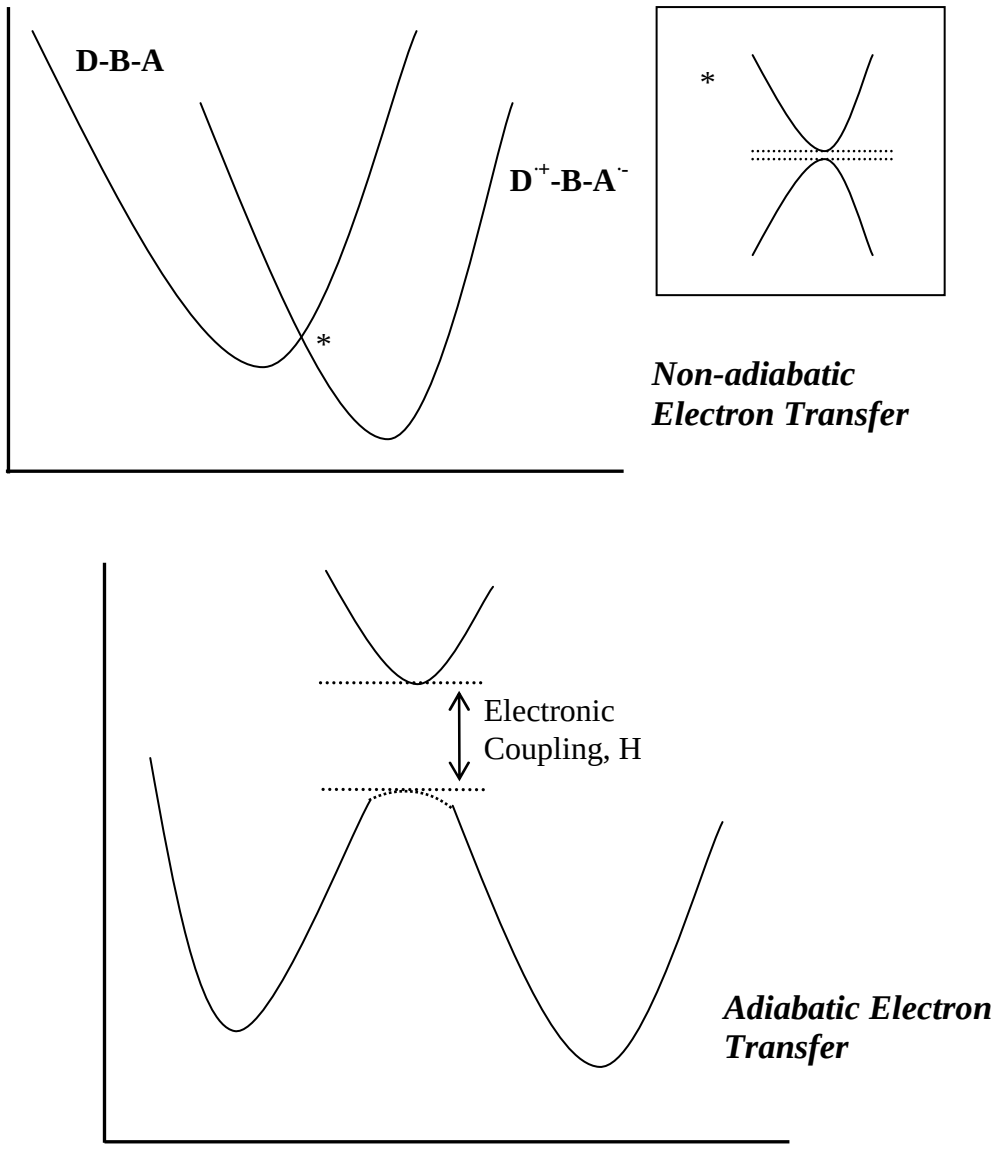

Figure 2.4: *Diagram of the non-adiabatic (top) and adiabatic (bottom) electron transfer processes. Adapted from reference 3.*

2.1.4.4 Heterogeneous Electron Transfer

The construction of interfacial supramolecular assemblies and the investigation of the associated electron transfer rates can aid in the understanding of the effects of different variables, including donor – acceptor distance, molecular structure, effects from the surrounding microenvironment etc., on the electron transfer process. The D-B-A model, in homogeneous electron transfer describes a system whereby both D and A are molecular species. This same donor – acceptor model can be used to describe heterogeneous electron transfer however, either the donor or acceptor species is now

an electrode depending on whether the electron transfer occurs in the form of oxidation or reduction of the molecular species at the interface. For this type of electron transfer to/from an electrode, the density of states within the electrode must be taken into account. The general idea is that for heterogeneous electron transfer to occur the donor state in the electrode must be matched energetically with a receiving state in the molecule (reduction) and *vice versa* for oxidation.

In heterogeneous electron transfer reactions at an electrode/solution interface, there are three individual steps involved in the overall electron transfer process. These include thermal activation of the energy levels within the donor and acceptor states, electronic coupling between the metal electrode and the reactant and the elementary electron transfer itself. Unfortunately the energies of molecular orbitals are not static in nature. Instead, they vary about a mean energy as a result of thermal fluctuations and the movement of solvent dipoles in the solvation shell. For electron transfer to occur the fluctuating donor and acceptor energy levels must resonate with each other.

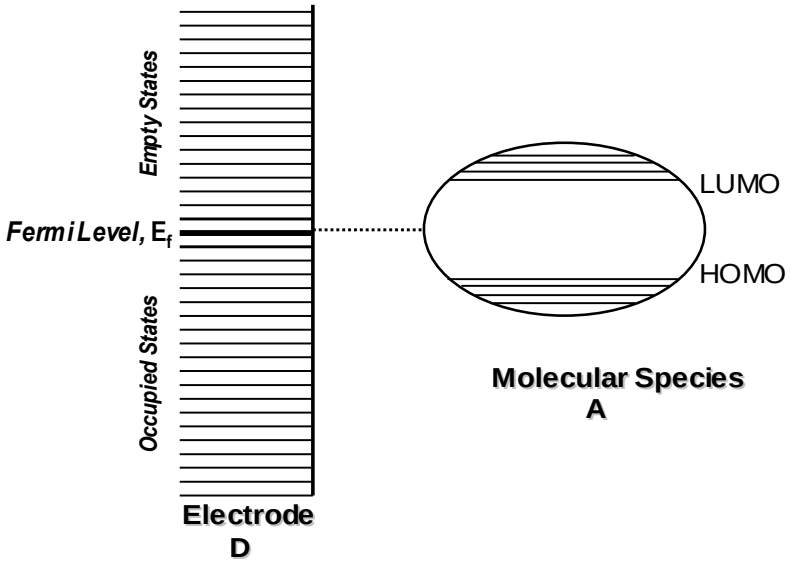

Figure 2.5: *Illustration of electronic states of a metal electrode and an adsorbed molecular species in an interfacial supramolecular assembly where heterogeneous electron transfer is possible. Adapted from references 2 and 3.*

Relying on thermal activation to induce electron transfer at the interface leads to a very low percentage of activated species at the electrode. Electronic coupling between the molecular species and the electrode is necessary following resonance between the electronic states. The shorter the distance between the electrode and the redox centre of the species at the electrode surface the stronger the coupling between the two. This coupling decreases exponentially with increasing distance.

Finally, the electron transfer step itself, as described above for homogeneous electron transfer, must adhere to the Franck Condon principle where the nuclear geometry of the molecule being oxidised or reduced does not change at the instance of electron transfer and the orientation of the solvent molecules in its solvent shell does not change. As a result, the internal structure of the energy levels of the reactant and product are the same. For adsorbed molecules, connected to the surface via a linker the electron transfer can occur via a superexchange or electron hopping mechanism involving the bridge. The difference between the two mechanisms is that in the case of the former, the energy levels of the bridge are off-resonance with those of the donor unit. This occurs when the bridge lies higher than the donor by 2 eV or more. The electron cannot travel across the bridge itself and instead the bridge facilitates electron transfer by extending the wavefunctions of the donor and acceptor units. Electron transfer takes place within a single step with the superexchange mechanism and the electron transfer rate experiences an exponential decrease with increasing length of the bridge. With the electron hopping mechanism the energy levels of the donor are in close resonance with those of the bridge and the electron can travel across the bridge in a series of steps. The electron transfer rate of the overall process is found from the sum of each individual electron transfer step from donor to acceptor via the bridge. The electron transfer for the hopping mechanism decreases inversely with increasing length of bridge.

Interfacial heterogeneous electron transfer processes are potential-dependent. The Fermi level, E_f corresponds to the highest occupied filled state, Figure 2.5. Changing the potential applied to the electrode alters the Fermi level: increasing to more negative potentials results in the Fermi level moving to a higher energy, whereas more positive potentials leading to a decrease in this energy. The heterogeneous electron

transfer rate is sensitive to the extent of electronic coupling between the reactant and the electrode. Adiabatic processes consist of electron transfer between strongly interacting reactants – occurring through states near the Fermi level of the electrode. The adiabatic potential-dependent rate constant is a function of both ν_N and the density of acceptor/donor states within the molecule. On the other hand diabatic electron transfer allows for the movement of electrons with energies below those of the states closely surrounding the E_f.[3]

2.1.5 Electrochemical Techniques

The diffusion controlled and surface confined properties of the compounds in this present thesis are characterised using voltammetric methods based on the linear sweep technique. These include cyclic voltammetry and differential pulse voltammetry, both of which are detailed in section 2.1.5.1 and 2.1.5.4 respectively.

2.1.5.1 Cyclic Voltammetry

Potential sweep methods provide a means of obtaining essential information about electrochemical reactions of chemical species in solution. Sweeping the potential with time, between an initial and final voltage, will result in well resolved current-potential curves. With potential sweep methods the signal is a voltage ramp where the potential is varied linearly with time. As the current is recorded against potential, and potential has a linear relationship with time it can be said that the current is essentially recorded against time.[2]

Increasing the potential linearly between an initial and final voltage is referred to as linear sweep voltammetry. Cyclic voltammetry operates on the same basis with the difference being that a reversal technique is employed whereby the potential is scanned back toward to the initial voltage, in the opposite direction, after reaching the final voltage, Figure 2.6. Analysis of the resulting cyclic voltammogram (CV) offers added information about the properties of the electrochemical reaction as well as any additional follow up chemical processes that may occur following electron transfer to or from the species involved.

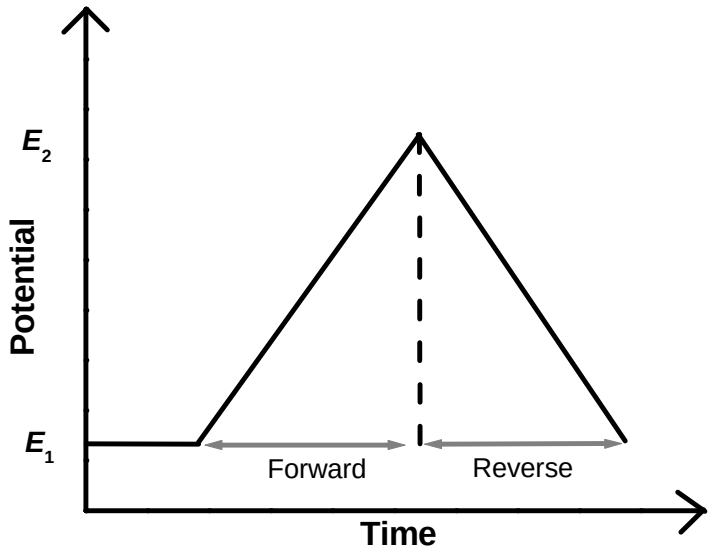

Figure 2.6: *Graph illustrating the potential-time relationship in a cyclic potential sweep.*

As the formal potential of the redox active species approaches, an increase in current is observed. As more of the compound is oxidised (or reduced depending on the applied potential) the surface concentration drops as there is less of the un-oxidised species in the double layer. When the potential moves beyond the formal potential, the surface concentration moves close to zero: mass transport of the redox active species has reached its maximum and as it declines the current begins to diminish. When the sweep direction is reversed the oxidised compound is reduced; providing that the scan rate is faster than the time taken for the species to diffuse away from the surface and there are no follow-up chemical processes occurring. A wave of opposite polarity is then observed. Two central characteristics of a CV are the peak potential, E_p and the corresponding peak current maximum, i_p.

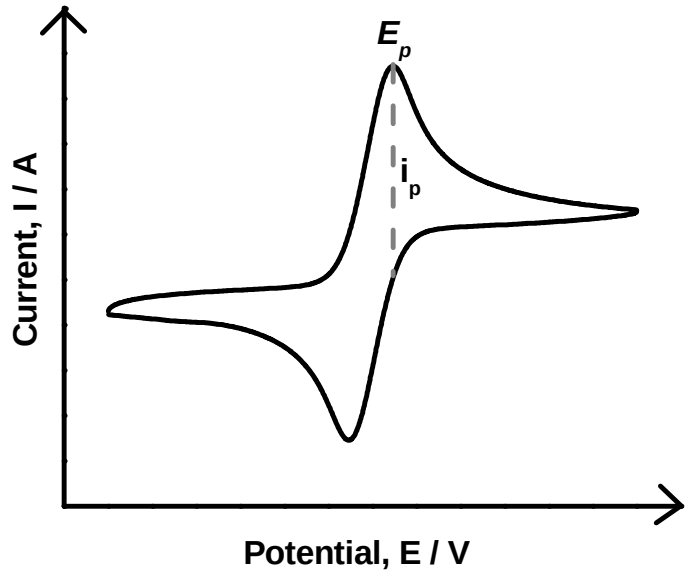

Figure 2.7: *A CV of a solution-phase redox couple showing the anodic peak potential and corresponding current.*

In solution phase electrochemistry the flux of an electroactive species, near an electrode surface is comprised of both migration and diffusion. The further from the electrode surface toward the bulk solution the greater the contribution from migration as the concentration gradient decreases. It is the flux of the oxidised or reduced species that controls the rate of reaction and hence the Faradaic current observed. Initially, at a potential where no Faradaic process can occur, it is purely the oxidised form of the redox couple present in the solution and the concentration is therefore uniform throughout. Applying a potential sufficient to reduce the species leads to the concentration at the electrode surface decreasing to zero and the further reduction of the oxidised species in the solution becomes a diffusion controlled state. Mass transfer of the electroactive species at the electrode becomes the rate determining step. A relationship between the flux and diffusion of the electroactive species with time is described using Fick's second law of diffusion (Equation 2.10).

Equation 2.10 $\Delta C_{(x,\,t)}/\Delta t = D\Delta C_{(x,\,t)}/\ \Delta x^2$

where C is the concentration of the electroactive species, x and t are the distance from the electrode surface, and the time the concentration gradient has existed respectively and D is the diffusion coefficient. A series of boundary conditions exist for Equation 2.10. Prior to the applied potential, at t = 0, and at distances at or near to the electrode surface the concentration of the electroactive species at the surface is the same as that of the bulk solution, C^b. When a potential is applied ($t \geq 0$), as the distance of the electroactive species from the electrode is being reduced to zero the concentration approaches that of the bulk solution. Finally, the concentration, at a zero distance from the electrode surface, is zero when the potential has been applied for $t > 0$.

At the electrode surface ($x = 0$) the diffusion gradient is related to the current, *i* by the Cottrell equation:

Equation 2.11 $$i = (nFAC^bD^{1/2}) / (\pi^{1/2} t^{1/2})$$

where *A* is the area of the electrode. Equation 2.11 can be applied to redox processes that involve semi infinite linear diffusion. This expression can be used in a variety of electrochemical techniques including polarography, voltammetry and controlled-potential electrolysis.

2.1.5.2 Reversible Redox Reactions – Solution Phase

For a kinetically reversible (Nernstian) electrochemical process the potential is related to the concentration of the electroactive species. Considering an electrochemical cell where an electroactive species (Ox) is reduced (Red) according to the following:

Equation 2.12 $$Ox + ne^- \leftrightarrow Red$$

The Ox and Red species are presumed to be at equilibrium at the electrode surface if rapid electron transfer kinetics accompanies the electron transfer process. The Nernst equation, (Equation 2.13) relates the half-cell potential of such a process to the concentrations of both species of the redox couple.

Equation 2.13 $E = E^o + (RT/nF)(\ln [Ox]/[Red])$

where E is the potential, E^o is the formal potential, R and T are the gas constant (J mol^{-1} K^{-1}) and temperature (K), n is the number of electrons transferred and F is the Faraday constant (C mol^{-1}).

For a reversible redox reaction, where diffusion of the electroactive species from the surface of the electrode is considered to be planar, according to the Randles-Sevcik equation, the peak current, i_p (A) may be expressed as follows:

Equation 2.14 $i_p = 2.69 \times 10^5 \, n^{3/2} A D^{1/2} C^b \nu^{1/2}$

where A is in cm^2, D is in cm^2/s, C^b is in mol/cm^3 and is in V/s. At 25º C the separation between the anodic and cathodic peak potentials, ΔE_p for a reversible process in solution is 0.059/n V in accordance with Equation 2.15.[2]

Equation 2.15 $\Delta E_p = E_{pa} - E_{pc} = 0.059/n$

Other relationships that lead to a solution phase redox reaction being qualified as reversible are the ratio of the anodic and cathodic peak currents being equal to unity, a linear dependence of the i_p with $\nu^{1/2}$, and a E_p that is independent of scan rate. Another useful parameter for characterising the voltammetric curve of a redox process is the half-peak potential, $E_{p/2}$. This is the peak potential at half the maximum i_p and is related to E_p as follows:

Equation 2.16 $E_p - E_{p/2} = 2.20 \, RT / nF = 0.0565 \text{ V } (25 ^\circ \text{C})$

Finally, the half-wave potential of a redox reaction, $E_{½}$ (V) is the average of the anodic and cathodic peak potentials. Under reversible conditions it may be related to the formal potential, E^o through Equation 2.17.

Equation 2.17 $$E_{½} = E^{o} + (RT/nF) \ln (D_{Red}/D_{Ox})^{1/2}$$

where D_{Red} and D_{Ox} are the diffusion coefficients of the reduced and oxidised species respectively. $E_{½}$ can be used as a decent estimate of E^{o} as D_{Red} and D_{Ox} are usually very similar in Nernstian reactions.

2.1.5.3 Reversible Redox Reactions – Surface Confined Properties

The electrochemical response of an adsorbed species Ox can differ significantly to that of the response of the same species in the solution phase. Considering a situation where Ox is adsorbed on an electrode surface where the amount of Ox in the solution phase is negligible (if present at all) and does not contribute to the Faradaic response. If the reduction of Ox, and the subsequent reoxidation is fully reversible the cyclic voltammogram for an ideal reversible surface adsorbed redox couple is given in Figure 2.8.

For an ideal reversible system the electroactive species Ox is reduced to the species Red and re-oxidised again. As this is a surface confined species and the electron transfer is not limited by diffusion, $E_{p,a} = E_{p,c}$ and the cyclic voltammogram consists of two redox waves that are symmetrical as $i_{p,a}$ is also equal to $i_{p,c}$.[2] The peak current is given by the following expression:

Equation 2.18 $$i_{p} = (n^2F^2/4RT)\, \nu A\Gamma$$

where n is the number of electrons transferred, ν is the scan rate (V/s), A is the area of the electrode (cm^2) and Γ is the surface coverage of the electroactive species (mol/cm^2). From Equation 2.18 there is a linear relationship between i_{p}, (and the current at any one point on the voltammetric curve) and ν. This is in contrast to the solution-phase where the i_{p} is dependent on $\nu^{1/2}$ for Nernstian diffusion controlled redox systems. As such, the linear dependence relationship between i_{p} and ν is a useful indicator of a surface confined species.

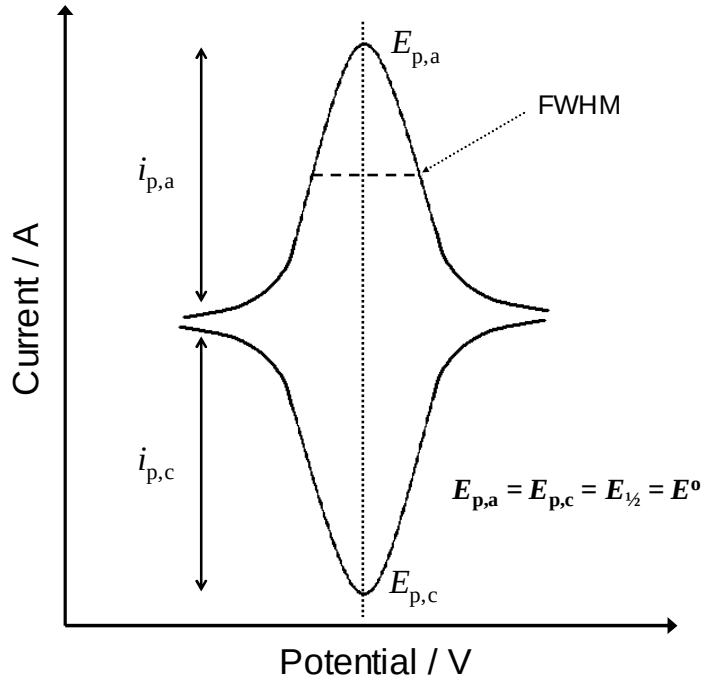

Figure 2.8: *Cyclic voltammogram of an ideal reversible surface confined redox process.*

Γ can be calculated from the cyclic voltammogram of the redox active species. The area under the wave corresponds to the charge associated with the reduction of Ox, Q (coulombs, C) and this can be related to the surface coverage, Equation 2.19.

Equation 2.19 $\Gamma = Q/nFA$

Surface confined species exhibiting close to ideal reversible redox behaviour under Langmuir conditions of adsorption (where there are no lateral interactions between adsorbates on the surface and $E_{p,a} = E_{p,c}$) will have a full width at half the current maximum (FWHM) for either the anodic or cathodic waves of 90.6/n mV (at 25º C). The FWHM deviates from this value when lateral interactions exist between adsorbates on the surface. Repulsive interactions lead to a FWHM > 90.6/n mV and attractive interactions produce FWHM < 90.6/n mV.

2.1.5.4 Differential Pulse Voltammetry

In contrast to potential sweep methods like linear sweep and cyclic voltammetry, differential pulse voltammetry optimises the ratio of the Faradaic current to the capacitive charging current, thereby increasing the sensitivity to the electrochemical response by sampling the current over a series of potential pulses in a staircase manner, Figure 2.9.

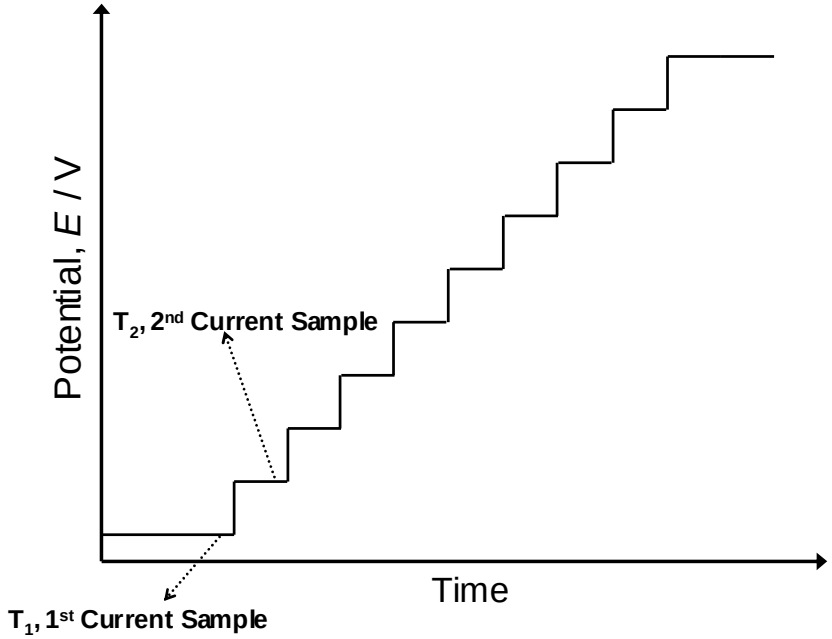

Figure 2.9: *Staircase waveform for differential pulse voltammetry where the current is measured before and after each potential pulse.*

A base potential is applied to the electrode and this potential is increased steadily by small amounts with each potential pulse. The change in potential with each pulse can range from 10 – 100 mV and the timescale between each change in potential is usually in the range of 5 – 100 ms.

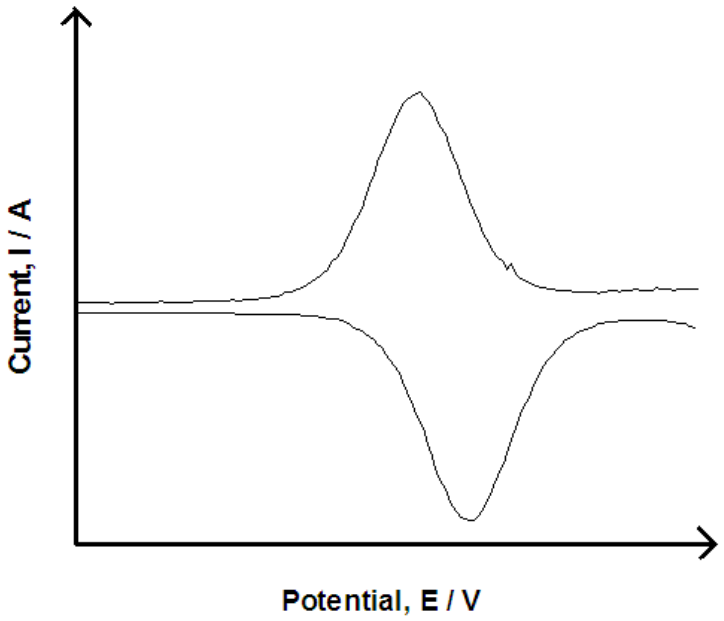

Figure 2.10: *Differential pulse voltammogram of a $Ru^{2+/3+}$ redox couple.*

Two current samples are taken for each pulse, the first of which is recorded at the end of each potential change just before the next one so that the contribution to the current signal from the capacitive charging current is minimized, Figure 2.9. Differential pulse voltammograms are a record of the difference between the initial and final currents of potential change against the base potential. A differential pulse voltammogram for a $Ru^{2+/3+}$ redox couple is shown in Figure 2.10.

2.1.6 Redox Chemistry of Ruthenium and Osmium Complexes

Ruthenium(II) and osmium(II) polypyridyl complexes are redox active species that give rise to stable oxidised and reduced forms. An interesting point to note with these metal complexes specifically is that the metal and ligand redox processes are generally fully reversible in the ground state. The stability and reversibility of these redox species is a fundamentally important requirement when considering these types of structures as potential building blocks for molecular electronic devices. $[Ru(bipy)_3]^{2+}$ is one of the most extensively studied ruthenium polypyridyl complexes in the literature. It is generally considered as a standard model and reference complex for comparing the redox chemistry of other ruthenium polypyridyl complexes. For this

reason the oxidation and reduction potentials of the complexes in this thesis are compared with those of $[Ru(bipy)_3]^{2+}$ and the corresponding osmium analogue, $[Os(bipy)_3]^{2+}$.

Above cryogenic temperatures (> -54º C) a typical CV of $[Ru(bipy)_3]^{2+}$ reveals a single reversible oxidation wave and three reversible reduction peaks. The oxidation of these complexes involves the removal of an electron from a metal centred orbital (Equation 2.20) giving rise to a M^{III} compound which has a low spin $\pi_M(t_{2g})^5$ configuration that is inert to ligand substitution.[13] Osmium polypyridyl complexes experience oxidation potentials that are approximately 400 mV lower than their ruthenium analogues. The reason for this is the slightly higher energy of the 5d orbitals of osmium compared to the 4d orbitals of ruthenium.[14] The higher energy of the orbitals leads to more polarizable electrons. These electrons in the 5d orbitals of osmium are less rigid than the corresponding electrons in the 4d orbitals of ruthenium and as a result less energy (lower oxidation potential) is required to remove an electron.

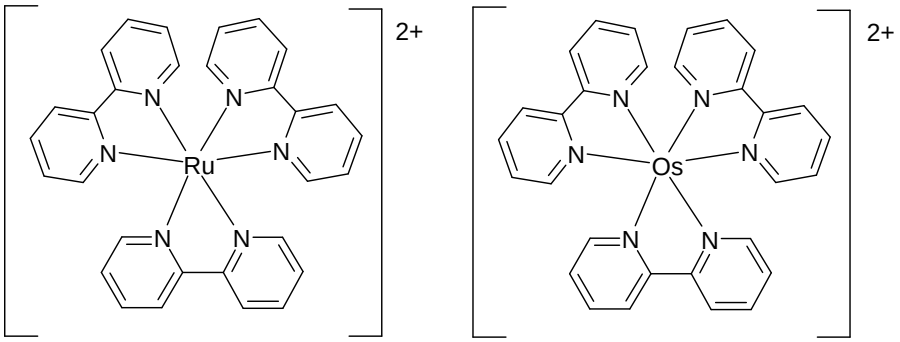

[Ru(bpy)$_3$]$^{2+}$ **[Os(bpy)$_3$]$^{2+}$**

Figure 2.11: *Molecular structures of the $[Ru(bipy)_3]^{2+}$ and $[Os(bipy)_3]^{2+}$.*

Reduction of ruthenium and osmium complexes (Equation 2.21) will involve the addition of an electron into a π^* orbital of one of the ligands providing the ligand field is strong enough to take preference over a metal centred reduction process (π_M^* (e_g) in octahedral symmetry).[15] As a result of the reduction occurring on the ligand the low spin $\pi_M(t_{2g})^6$ configuration is retained and therefore the reduced form is generally reversible and inert to ligand substitution. At room temperature no more than a single

electron is placed on each of the bipyridyl units. However, at cryogenic temperatures (-54º C), using dimethylformamide as the electrochemical solvent it is possible to add up to six electrons to the complex which may be assigned to successive first and second reductions of each bipy unit.[16] This yields the complex: $[Ru^{II}(bipy^{2-})_3]^{4-}$.

Complex	Metal Oxidation Potential [V]	First Ligand Reduction Potential [V]
$[Ru(bipy)_3]^{2+}$	+1.26	-1.35
$[Os(bipy)_3]^{2+}$	+0.83	-1.28

Table 2.1: *Redox potentials of $[Ru(bipy)_3]^{2+}$ and $[Os(bipy)_3]^{2+}$ (vs. SCE).*[14]

Oxidation:

Equation 2.20 $[M^{II}(L)_3]^{2+} \rightarrow [M^{III}(L)_3]^{3+} + e^-$

Reduction:

Equation 2.21 $[M^{II}(L)_3]^{2+} + e^- \rightarrow [M^{II}(L)_2(L^-)]^+$

The redox potential of the metal centred oxidation can vary depending on the nature of the coordinated ligands. Those ligands with strong σ-donor or weak π-acceptor capabilities, e.g. triazole ligands or Cl^- ions, will donate electron density to the metal centre thereby lowering the oxidation potential: $[Ru(bipy)_2Cl_2]$ is oxidised at +0.35 V [17] in acetonitrile, *vs.* SCE. In contrast, strong π-acceptor or weak σ-donor ligands, e.g. bipyridyl rings or CO ligands, will increase the oxidation potential of the metal centre as a result of less electron density on the metal centre: $[Ru(bipy)_2CO_2]^{2+}$ is oxidised at potentials greater than +1.9 V [18] in acetonitrile, *vs.* SSCE. As well as the coordination sites, other factors that can influence the oxidation potential of metals include steric and electronic effects.

2.2 Electronic Properties of Transition Metal Complexes

Transition metal complexes consist of metal centres coordinated to neutral or anionic ligands. These two components can also exist independently from the other and for this reason localized molecular orbital (MO) diagrams can be used to outline the ground state, excited states and redox states of coordination complexes, Figure 2.12. Molecular orbital theory, in its simplest form, deals with the idea that the overlap of the outer orbitals of two atoms can create a chemical bond in such a manner that the electron density between the cores of each atom is shared. In such diagrams each molecular orbital is assigned as being metal (M) or ligand (L) based depending on its predominant location, i.e. whether the greater contribution comes from the metal or the ligand.

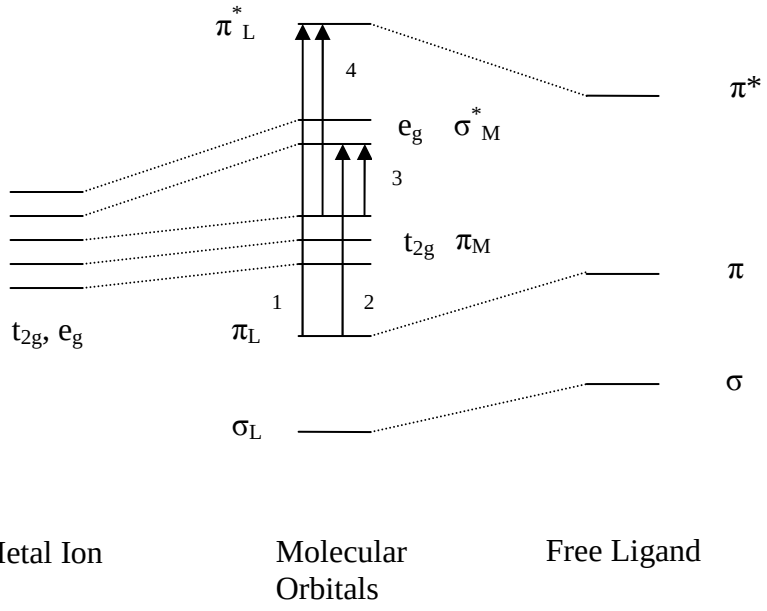

Figure 2.12: *Jablonksi diagram outlining the metal and ligand orbitals and the possible electronic transitions in an octahedral ligand field transition metal complex. 1) Ligand centred transition from the ligand $\pi \rightarrow \pi^*$ orbitals. 2) Ligand to metal charge transfer; ligand $\pi \rightarrow d^*$ orbital of the metal. 3) Metal centred transition from the metal $d \rightarrow d^*$ orbitals. 4) Metal to ligand charge transfer; metal $d \rightarrow \pi^*$ orbital of the ligand.*

The ground electronic configuration of transition metal complexes in their most common oxidation state, e.g. ruthenium(II) and osmium(II) complexes, have filled σ_L

and π_L orbitals and partially or completely filled π_M orbitals. Any orbitals of higher energy are usually empty in the ground state. However, redox and light absorption processes can affect the orbital populations by moving electrons from one orbital to another, thereby giving rise to different molecular orbital formations for each redox and excited state.

The relative energies of the transitions involved in the ligand centred (LC) process, also known as intraligand (IL), labelled 1 in Figure 2.12, will be equivalent to those of the corresponding processes occurring in the free ligand. Ligand to metal charge transfer (LMCT) involves the distribution of electron density from a coordinated ligand to the metal centre t_{2g} orbitals where the ligand is formally oxidised and the metal centre reduced. In contrast to this ligand dominated process, metal to ligand charge transfer (MLCT) involves the movement of an electron from a metal based MO to that of a ligand centred MO resulting in stabilisation of the metal orbitals. With this type of transition the metal centre is formally oxidised with the loss of electron density and the ligand based MO is reduced. Finally, the metal centred transitions are comprised of the movement of electron density from the t_{2g} to the e_g orbitals – rearrangement of charge between the d orbitals of the metal complex.

In the localised MO approach oxidation is generally considered as the removal of a metal localized electron with reduction being the addition of an electron to a ligand π^* orbital. In octahedral transition metal complexes the highest occupied molecular orbital (HOMO) is normally metal centred whereas the lowest occupied molecular orbital (LUMO) can be metal or ligand centred. In most cases the ligand field is strong resulting in reduction taking place on the ligand.

2.2.1 Electronic Absorbance Spectroscopy

Absorption spectroscopy is concerned with the interaction of photons (i.e. $h\nu$) with molecules in solution and the perturbations created within the molecule following this interaction. Several electronic states exist within molecules, each of which have a different associated energy. Absorption of a photon will occur only when this photon of light possesses an energy that is equal to the energy gap between two of these electronic states (e.g. $S_0 \rightarrow S_1$, Figure 2.13) within the molecule. When this occurs,

the internal energy of the molecule is increased and the system moves from the ground state to a *photo-excited state*. With the promotion to an excited state comes an increase in energy of the molecule - it is energetically unstable. This excess energy is then dispelled in a variety of different ways including loss of heat, emission of a photon or a proceeding chemical reaction.

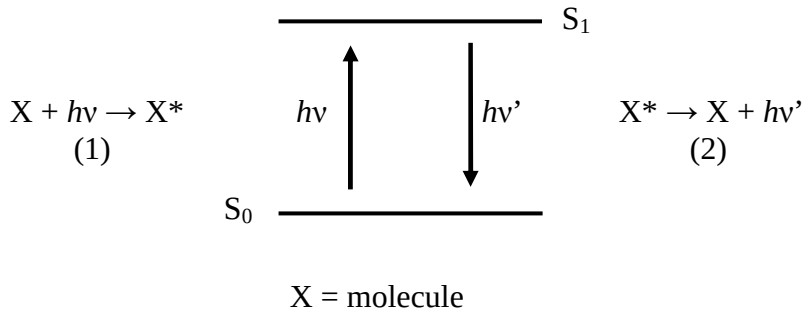

Figure 2.13: *Illustration of the input and output of a photon between different energy levels of a molecule during absorption (1 – left) and emission (2 – right).*

Electronic absorption of a photon by a molecule involves a rearrangement of electron density rather than simply promotion of a single electron from the HOMO to the LUMO. Several vibrational states exist within the ground state of a molecule as a result of continuously changing bond lengths, i.e. the ground state is not static. Transitions from the ground to the excited state occur at a very fast rate. Within this timescale the nuclear geometry (bond lengths and angles) of the molecule does not change and the excited state is said to be identical to that of the ground state. This temporary state bearing the same bond lengths and angles as the ground state is referred to as the Franck-Condon state (as previously discussed in section 2.1.4.1).[19] More than one Franck-Condon state may exist as a result of several vibrational levels in the ground and excited states and therefore several transitions are possible. The wavefunction of each vibrational level of the ground state will overlap to an extent with a wavefunction of one of the vibrational levels of the excited state, e.g. $S_{0,\,v=0} \rightarrow S_{1,\,v=2}$ (Figure 2.14).[20] However, it is the transition that involves the most overlap between wavefunctions of a ground vibrational level with that of an excited state vibrational level that will have the highest probability of occurring.

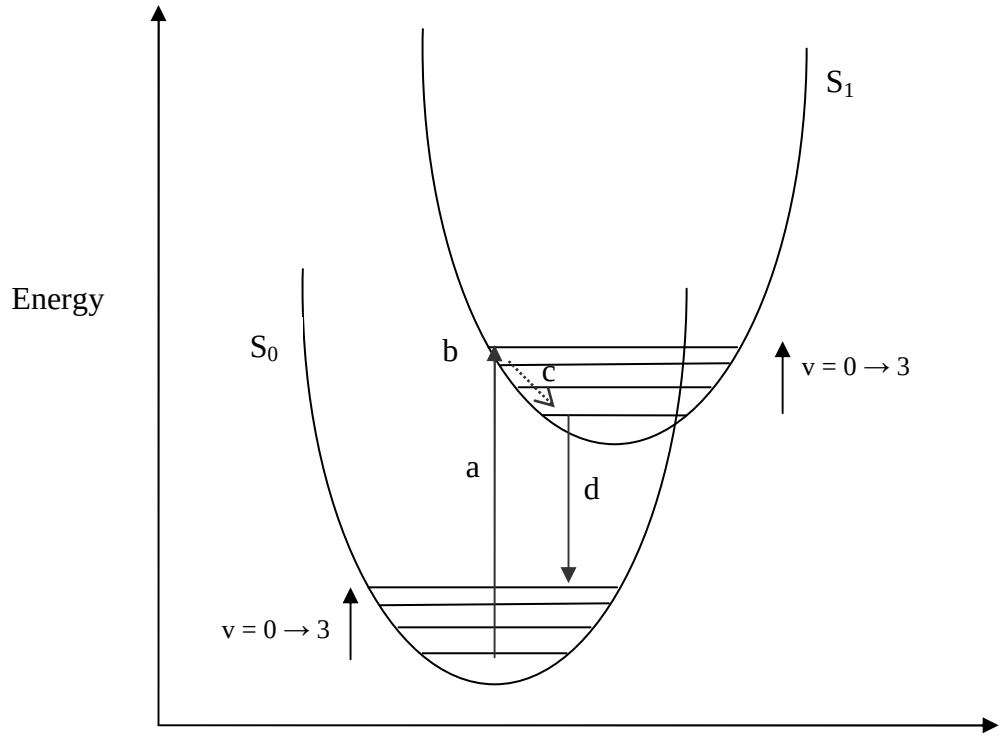

Figure 2.14: *Potential well diagram of a ground state (S_0) and the excited state (S_1) following absorption of a photon. The diagram is used to illustrate a. absorption, b. Franck-Condon state, c. vibrational relaxation to the lowest vibrational level of the excited state and d. emission (fluorescence). Adapted from reference 20.*

The Franck-Condon principle also suggests that these types of electronic transitions are vertical in nature as a result of negligible change in the nuclear geometry of the excited state with respect to the ground state.[19] The shape of the absorbance spectrum arises as a result of the different probabilities of each possible electronic transition.

2.2.2 Luminescence

Once a molecule is in an electronically excited state the excess energy associated with that state renders it energetically unstable. In order to dissipate this excess energy several processes can occur, Figure 2.15. Provided there are no other molecules around with which the excited molecule can interact, these follow-up processes consist of fluorescence, phosphorescence, dissociative bond breaking and non-radiative decay.

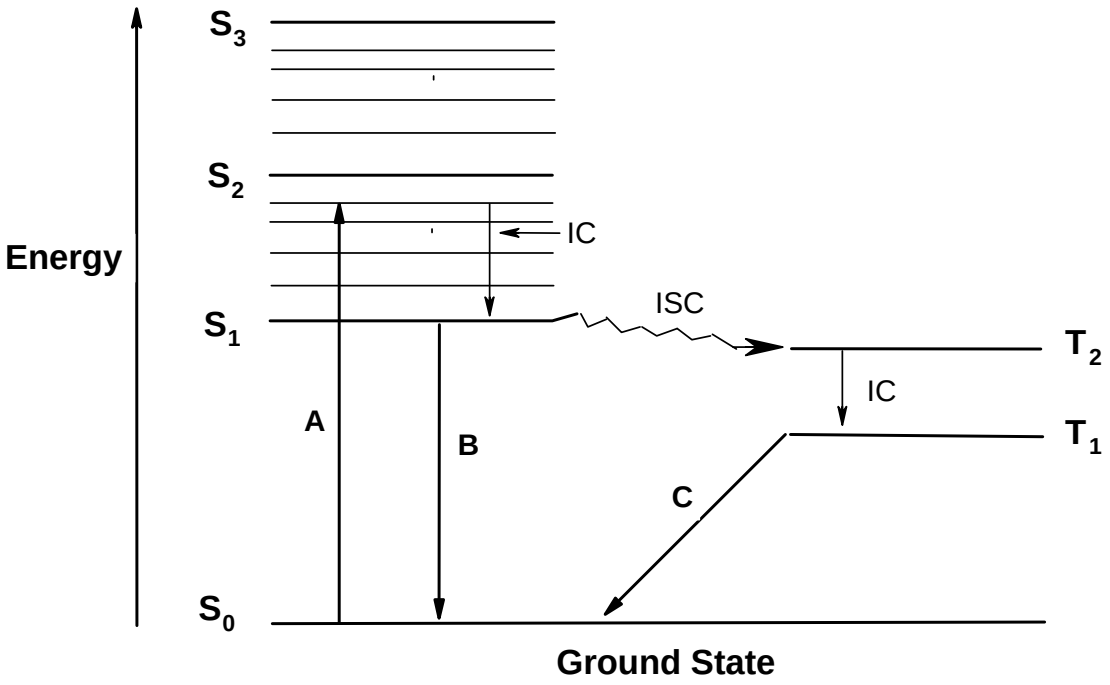

Figure 2.15: *Jablonski diagram detailing the possible routes of decay following absorbance of a photon (A): the luminescence pathways are indicated by B – fluorescence and C – phosphorescence. IC represents internal conversion (vibrational cooling) and ISC indicates intersystem crossing from the singlet to the triplet state.*

Luminescence (fluorescence and phosphorescence) consists of the emission of a photon from the lowest vibrationally excited state to the ground state, Figure 2.13. Kasha's rule states that fluorescence occurs by a transition from the lowest vibrationally excited singlet state ($S_{1,\ v\ =\ 0}$), to a vibrational level in the ground state ($S_{0,\ v\ =\ n}$).[21] This photon is of lower energy than the photon of absorbance as a result of the loss of energy due to the vibrational relaxation to the lowest excited state, which possesses different nuclear coordinates to that of the ground state. This energy difference is known as the Stokes shift, i.e. the difference in energy between the λ_{max} of absorption and the λ_{max} of emission. As is the general rule concerning the probability of different absorption transitions, the same idea applies to fluorescence: the most probable transition from the excited state to the ground state will be that of the greatest overlap of an excited state wavefunction with a corresponding wavefunction of the ground state.

The existence of the phenomenon known as spin-orbit coupling (which arises in molecules with heavier atoms as a result of the interaction of the electron's spin angular momentum with the orbital angular momentum) allows for the usually forbidden process known as intersystem crossing (ISC) to occur, Figure 2.15. This involves the conversion of the singlet (S_1) excited state to the triplet (T_1) excited state which has a different spin multiplicity. Radiative decay may then occur from the T_1 state back to the ground state and this type of emission is known as phosphorescence. As you move down a group in the periodic table to heavier atoms the probability and degree of ISC to the T_1 state increases as a result of increased spin-orbit coupling. Therefore phosphorescence is more common in molecules incorporating these heavier atoms. The lifetimes of phosphorescent emission processes are quite long with times varying over a range of 10^{-7} to 10^{-3} sec. Fluorescence occurs at a much faster rate and is within the range of 10^{-12} to 10^{-10} sec.

2.2.3 Electronic Properties of $[Ru(bipy)_3]^{2+}$

Several bands are observed in the absorbance spectrum of the parent ion $[Ru(bipy)_3]^{2+}$.[15, 22] Comparing this spectrum with that of the free protonated bipyridyl ligand allows for the assignment of the two high energy intense bands, in the UV region at 185 and 285 nm, as LC π-π^* transitions.[23] ^{1}MLCT absorbance bands are present in the spectrum at both 240 and 450 nm. These represent charge transfer transitions from a ruthenium metal centred *d* orbital to the π^* orbitals of the bipyridyl unit. The absorbance bands at 322 and 344 nm are tentatively assigned to metal centred transitions. At low temperatures (77 K) an additional band is observed further into the visible region of the spectrum at 550 nm which may be assigned to the spin-forbidden ^{3}MLCT transition.[24]

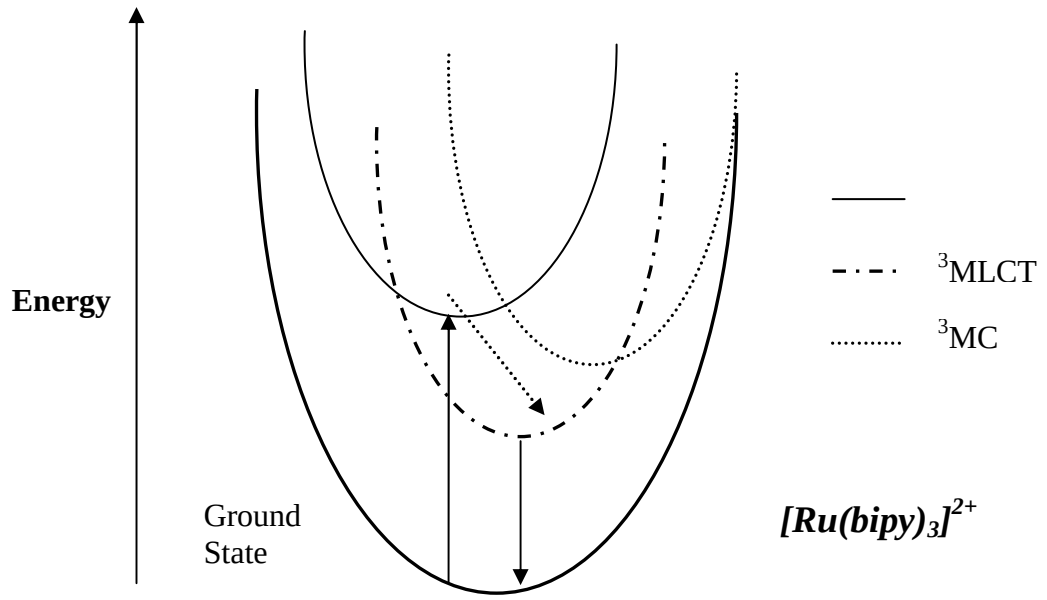

Figure 2.16: *Illustration of the ground and excited states of $[Ru(bipy)_3]^{2+}$. The solid arrows represent the radiative absorption and emission processes where the dashed arrow represents ISC.*

In the earlier days following on from the initial report of luminescence from $[Ru(bipy)_3]^{2+}$ reported by Paris and Brandt [25] a large degree of ambiguity surrounded the nature of this luminescence. Agreeing with the results from Crosby and Demas [26] in 1968, Lytle and Hercules [23] elucidated the pathway of luminescence as the spin-forbidden phosphorescent process that is charge transfer in nature, i.e. $[Ru^{II}(bipy)_3]^{2+} \rightarrow [Ru^{III}(bipy^{-})(bipy)_2]^{l2+}$. It is suggested that ISC allows for a spin-forbidden luminescence (lifetime of 5 μs at 77K in rigid alcoholic glass) that is ^{3}MLCT in nature involving a single ligand localized excitation, i.e. the excited electron inhabits a single bipy ligand and not a delocalized π* orbital.[15] The ^{3}MC excited state can also be populated (thermal process). It is this population that determines the photo stability of the complex in the excited state.[27]

2.3 Raman Spectroscopy

Several spectroscopic techniques are now available for the characterisation of the electronic structure and properties of molecular systems both as free species and when

bound to a surface. Vibrational spectroscopy is of particular interest as it provides additional structural information based on the vibrational modes within a complex that is complimentary to other techniques used such as UV/Vis spectroscopy or electrochemistry. Raman spectroscopy is a technique employed to investigate low frequency vibrational and rotational modes in a molecule. This method works on the basis that when light from a laser (in the UV/Vis or NIR range) hits a molecule, inelastic scattering (Raman scattering) of that light incident on the molecule occurs. This is as a result of the interaction between the light and the different vibrational modes within the system. Energy between the incoming photon of light and the molecule is exchanged which leads to the inelastic scattering of the light, Figure 2.17.[28] The molecule is now said to be in a virtual energy state which then relaxes to a vibrationally excited state.

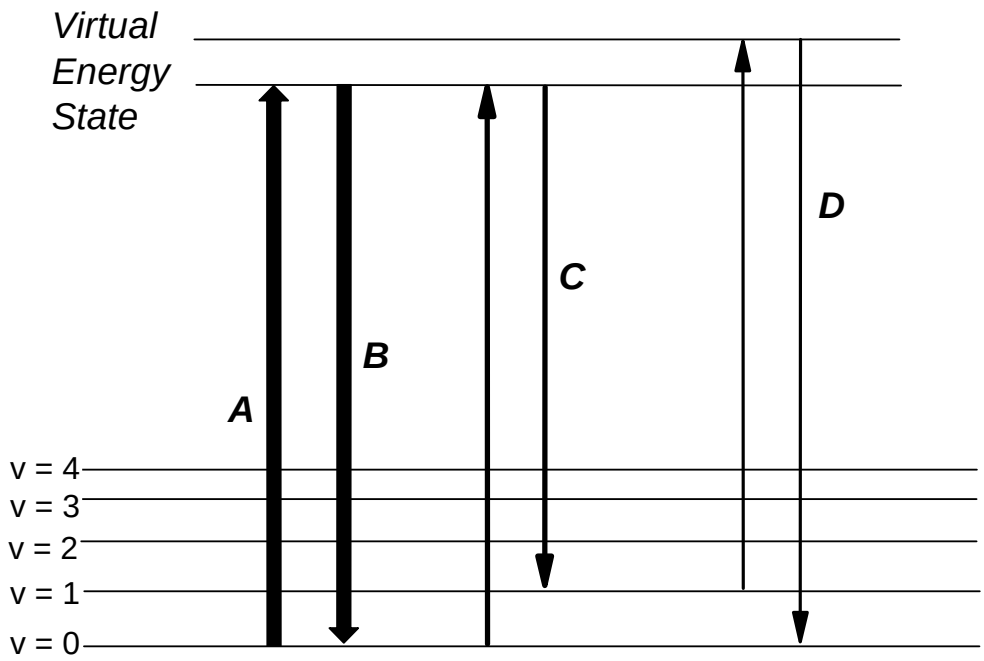

Figure 2.17: *Illustration of the possible types of scattering in conventional Raman spectroscopy:* ***A*** *corresponds to the incident excitation photon with a photon of the same frequency emitted* (***B***) *due to Rayleigh scattering; Stokes scatter* (***C***) *where the energy of the photon is less than the incident photon and* ***D****, the anti-Stokes scatter where the energy of the emitted photon is greater than the incident photon.*

Following the collision between the laser and the molecule, a second photon of light is emitted which has a different frequency, ν to the incident photon, ν_0. The second photon may have a frequency that is greater or less than that of the incident photon. Where this Raman scattered photon has a frequency that is greater than the incident photon, i.e. $\nu + \nu_0$, this becomes known as the anti-Stokes Raman scatter. The Stokes Raman scatter therefore, is the opposite case where the frequency of the scattered photon is less than the incident photon, i.e. $\nu + \nu_0$. Regardless of whether the scattered photon is bigger of smaller, the difference between the two, $\Delta\nu$ represents the vibrational quanta in the molecule. It must noted that the intensity of the signal from spontaneous Raman scattering is incredibly weak with only 1 in 10^8 to 10^{11} molecules within the analyte sample scattering inelastically.

A room temperature, the vibrational level, $v = 0$ has the highest probability of being populated. Therefore, in Raman spectroscopy, the most likely process is that of Stokes scatter, ***C*** in Figure 2.17: this originates from the $v = 0$ level and the release of the scattered photon prompts the molecule to relax back to higher $v = 1$ level (emitted photon of less energy than the incident photon). There is less chance of the weaker anti-Stokes process occurring as the $v = 1$ level is rarely populated at room temperature. For molecules to be Raman active the ability to polarize the molecule, i.e. create a change in the electron density within the molecule, with respect to the vibrational coordinate is required. Asymmetric molecules are favoured in Raman spectroscopy. Molecules such as H_2O and other highly polar systems tend to be harder to polarize and as a result give very weak Raman signals.[28]

The fact that only 1 in 10^8 to 10^{11} molecules will scatter inelastically results in a very weak Raman signal. This can be overcome by using a technique known as resonance Raman. Using a laser that has an excitation wavelength equal to that of the electronic absorption band of the molecule allows for a much greater enhancement of the Raman signal associated with the excited electronic state (can be increased by a much as a factor of 10^6). This is as a result of the resonance enhancement of the scattering from the vibrational modes associated with that electronic transition specifically. The electronic transitions within the molecule can be investigated using this technique as the vibrational bands associated with each transition are selectively enhanced.[29]

Other Raman techniques that will be briefly discussed within this thesis include excited state Raman spectroscopy where the molecule is bombarded with the laser of appropriate wavelength and promoted to an electronically excited state. Raman spectroscopy is then used to monitor the vibrational modes of the molecule in the excited state. Surface enhanced Raman spectroscopy (SERS) is also used to investigate the structure of molecules when bound to a surface. This is normally carried out on a Au or Ag surface or alternatively Au or Ag colloid can be used. The enhancement of the Raman signal for the molecule on the surface arises as a result of the greater electric field created by exciting the Au or Ag particles with the laser. The intensities of the signals are proportional to the electric field within and therefore enhancement of the surface confined molecular vibrational modes occurs. Increased interest in SERS rose from the first investigations in the 1970's where the surface Raman spectrum of pyridine was obtained.[30] Although it was not realised at the time, this was in fact the first SERS spectrum and opened up a new method of characterisation for the world of surface science.

2.4 Experimental Methods

2.4.1 Electrochemical Cell Setup

In Chapters 3 through to 6 in this thesis, all cyclic voltammetry and differential pulse voltammetry experiments of the solution phase and surface confined complexes were carried out using a three electrode cell setup. The three electrodes consist of the working, reference and counter (auxiliary) electrodes, Table 2.2. The potential is measured between the working and reference electrodes with the current passed between the working and counter electrodes. It is important that the counter electrode does not interfere with the working electrode, i.e. it must not produce any species that may approach the working electrode and interfere with the electrochemical reactions taking place there. The reference electrode is a non-polarizable electrode in that its potential does not vary from its open-circuit value as negligible current is drawn through it. However, the potential measured between the working and reference electrodes includes a potential drop. The resistance of the solution (between the working and counter electrodes) is a function of the potential (or *i*) and as such this

potential drop is a product of the current and resistance of the solution and is known as the *iR* (Ohmic) drop.[2]

The placement of the reference electrode in the electrochemical cell is important when trying to minimise the *iR* drop of the solution. A certain amount, but not all, of the *iR* drop is accounted for by the electrochemical potentiostat and ideally, the reference electrode should be placed as near to the working electrode as possible to minimise the contribution to the measured potential from the uncompensated resistance, R_u. At a planar working electrode, where the current densities across its surface are uniform and not shielded by the reference electrode, the uncompensated resistance can be expressed as shown in Equation 2.22.[2]

Equation 2.22 $R_u = x/\kappa A$

where x is the distance between the working and reference electrodes, κ is the solution conductivity and *A* is the area of the working electrode.

Electrode	**Type Used**
Working	Platinum (Pt) Gold (Au) Glassy carbon (GC)
Counter	Pt wire
Reference	Saturated calomel electrode (**SCE**) in saturated KCl Mercury/mercury sulphate (**Hg/HgSO$_4$**) in saturated K_2SO_4 Silver/silver chloride (**Ag/AgCl**) in 3M KCl Silver/silver ion (**Ag/Ag$^+$**) in 0.01M Ag^+ solution* Ag wire

Table 2.2: *Details of each different working, counter and reference electrodes used in this thesis. * 0.01 M Ag^+ solution is made up of 0.01 M $AgNO_3$ and 0.1 M of the electrolyte to be used in the experiment. The solvent used to make up the solution is that of the electrolyte solvent used for that particular experiment.*

Pt and Au electrodes are commonly used in electrochemistry. Both of these metals can be obtained in high purity and can be fabricated into different geometric configurations for the construction of electrodes. However, these metals are not entirely inert. Pt has quite a small overpotential for hydrogen evolution whereas Au does not appreciably adsorb hydrogen - it has a larger overpotential for hydrogen evolution. Cyclic voltammetry in sulphuric acid, *vide infra*, using a Pt electrode reveals hydrogen adsorption and desorption peaks whereas these are absent from the CV obtained for the same experiment using Au, Figure 2.18. Both of these metals form an oxide layer, in aqueous electrolyte at anodic potentials, which is considered to be formed by oxygen being chemisorbed on the surface leading to a metal-oxide film. This oxidation of the metal surface occurs at more positive potentials for Pt compared to Au and in polar aprotic solvents the oxide layer is less pronounced allowing for a more positive potential window. The third material used as a working electrode in this thesis is the electrically conductive glassy carbon (GC) electrode. This material can be obtained in a pure state and is quite resistant to chemical attack. It has a larger overpotential for the production of hydrogen compared to Pt or Au.

Prior to analysing an electroactive species, the working electrodes need to be cleaned. All three electrodes, Pt, Au and GC, were manually polished using an alumina slurry. This was done by holding the electrode parallel to a polishing pad and gently moving it using a ‘figure of 8’ mechanism. The alumina slurry is made by mixing aluminium oxide powder (1.0, 0.3 or 0.05 µm, CH Instruments , Inc.) with water. The electrodes were sonicated in deionised water for 5 minutes after each successive polishing with each grade of alumina slurry. The GC electrode was sonicated in the appropriate electrochemical solvent following polishing.

In addition to manual polishing, both the Pt and Au electrodes were cycled in 0.5 M H_2SO_4 as electrochemical cleaning in acid ensures that all contaminants are removed from the surface of the electrode. A $Hg/HgSO_4$ reference electrode was used to minimise any contamination from chlorine which can affect the pre-treatment process. Figure 2.18 includes cyclic voltammograms of both Pt and Au electrodes in 0.5 M H_2SO_4. The waves associated with the Pt and Au oxide formation and reduction are indicated in each CV, as are the hydrogen adsorption and desorption peaks.

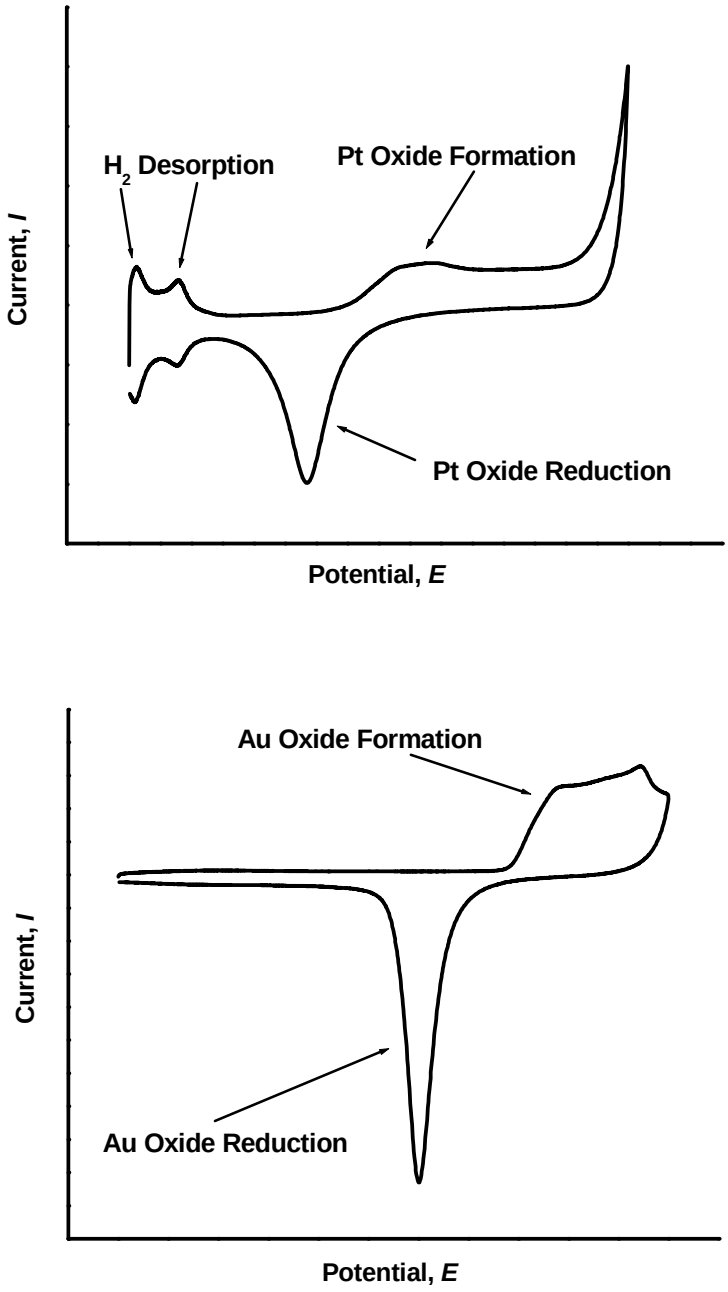

Figure 2.18: *Cyclic voltammograms of a Pt (top) and Au (bottom) electrode (2 mm diameter), vs. Hg/HgSO₄, in 0.5 M H_2SO_4.*

In Chapter 3, Au bead electrodes were used as the substrate for the formation of monolayers of the complexes discussed therein. Prior to deposition the bead was cleaned via manual cleaning accompanied by electrochemical cleaning. The manual cleaning consisted of a Au bead connected to the anode of a 3 V battery using Pt wire and the bead is then placed in a beaker containing 0.5 M H_2SO_4. A second Pt wire is

then placed in the same container to complete the circuit. Following oxidation of the Au (bead turns a rustic orange/brown colour) the electrode is then immersed in 1 M HCl prior to electrochemical cleaning in 0.5 M H_2SO_4 using the method described above.

The Pt electrodes were cycled between -0.6 and 1.0 V (*vs.* $Hg/HgSO_4$) for 21 sweep segments or until a stable state was achieved where no further increases were observed in the current density of the metal-oxide peaks. As the Au oxide layer forms at potentials less positive than Pt the Au electrodes were cycled between -0.1 and 0.9 V (*vs.* $Hg/HgSO_4$). The area under each Faradaic wave in the CV is representative of the charge associated with that process (after subtraction of the background charging current). The charge associated with the reduction of the Pt oxide layer is used to calculate the real surface area of the electrode.[31] The standard value for the surface oxide charge per unit area for each metal (Q_{sa}) is 420 x 10^{-6} C/cm^2. Using this value and the charge of the metal oxide reduction peak (Q_{ra}), the real surface area of the metal electrode can be calculated using the following expression:

Equation 2.23: $$A_r = Q_{ra} / Q_{sa}$$

where A_r is the real surface area of the electrode in cm^2.

2.4.2 Experimental Conditions

2.4.2.1 Cyclic Voltammetry and Differential Pulse Voltammetry

Electrochemical experiments were carried out using CH Instruments Version 8.15 software controlled electrochemical bipotentiostat (CHI750C). Unless otherwise stated, typical concentrations of 1 mM were used for solution phase electrochemical measurements throughout. A Pt wire was used as the counter electrode. The working and reference electrodes used in this thesis are detailed in Table 2.2.

A list of the electrochemical solvents and electrolytes is given in Table 2.3. The principle solvents used for diffusion-controlled cyclic and differential pulse

voltammetry were acetonitrile and dichloromethane. A 50:50 mix of both of these solvents was used as the electrochemical solvent in Chapter 4 to avoid adsorption on the electrode surface. Sulphuric acid (Aldrich, 99.999%) was used for the pre-treatment of the electrodes.

When investigating cathodic processes and scanning to negative potentials the electrochemical cell was degassed for at least 10 minutes using argon and a blanket of argon was maintained throughout the experiment. This was to ensure that all oxygen was removed from the solution prior to reducing the complex. Cyclic voltammograms were recorded at a scan rate of 100 mV/s, unless otherwise stated. The experimental error involved is ± 30 mV.

Electrolyte Salt	**Source**	**Solvent**	**Source**
Tetrabutylammonium Hexafluorophosphate ($TBAPF_6$)	Fluka, electrochemical grade ≥ 99.0 %	Acetonitrile (ACN)	Aldrich anhydrous, 99.8%
Tetrabutylammonium Tetrafluoroborate ($TBABF_4$)	Fluka, electrochemical grade ≥ 99.0 %	Dichloromethane (CH_2Cl_2)	Aldrich, anhydrous, 99.8 %
Tetrabutylammonium Perchlorate ($TBAClO_4$)	Fluka, electrochemical grade ≥ 99.0 %	Dimethylformamide (DMF)	Aldrich, spectrophotometric grade, 99.8%
Lithium Perchlorate ($LiClO_4$)	Aldrich, 99.99 %	Propylene Carbonate	Aldrich, Anhydrous 99+ %
		Tetrahydrofuran (THF)	Aldrich, HPLC grade 99.9%
		Ethanol (EtOH)	Breanntag, GPR grade
		Acetone	Cooley Distillaries, GPR grade

Table 2.3: *Details of the origin and grade of the different electrochemical solvents and electrolytes throughout this thesis.*

2.4.2.2 Monolayer Formation

Monolayers of four transition metal complexes (Chapter 3) and an organic compound (Chapter 5) have been formed. The procedure used for the formation of the monolayers was that of solution-phase deposition. This technique consists of pre-treating Pt macro and Au macro and bead electrodes using the appropriate method described in section 2.3.1. The clean metal electrodes were then immersed in a solution of the surface active molecule for a period of 24 hours. The concentration of the solutions used for the immersion of the electrodes was typically 500 µM unless stated otherwise. The solvent composition of the deposition solvents used for the compounds in Chapters 3 and 5 is detailed in Table 2.4.

Surface Active Species	Deposition Solvent
Ru(pyrphen)	DMF/H_2O (1:1)
Os(pyrphen)	DMF/H_2O (1:1)
Ru(thimphen)	EtOH
Os(thimphen)	EtOH
dipyrBEDT-TTF	DMF/H_2O (9:1) and CH_2Cl_2

Table 2.4: *Surface active species and their deposition solvents for monolayer formation.*

Several solvent system and concentrations were used for the organic compound, dipyrBEDT-TTF due to poor adsorbance of the species on the substrate surface. This is discussed in more detail in Chapter 5.

2.4.2.3 Oxidative Spectroelectrochemistry

The oxidative spectroelectrochemistry detailed in Chapters 3, 4 and 5 was carried out in the University of Groningen, under the supervision of Dr. W.R. Browne. JASCO 630 UV-Vis and 570 UV-Vis/NIR spectrophotometers were used to record the UV-Vis/NIR data. The potentials were controlled using bulk electrolysis on a model CHI760C potentiostat (CH Instruments, Inc.). Analyte concentrations were typically 0.5-1.0 mM. In Chapters 3 and 4 the electrolyte was made up of anhydrous acetonitrile containing 0.1 M tetrabutylammonium hexafluorophosphate ($TBAPF_6$).

Platinum gauze working electrode, Pt wire counter electrode and SCE reference electrode were employed (calibrated externally using 0.1 mM solutions of ferrocene in 0.1 M $TBAPF_6$ in acetonitrile). In Chapter 5 the electrochemical solvent was dichloromethane and a Ag wire was used as the reference electrode. As for the previous two chapters, a Pt wire and Pt gauze were used as the counter and working electrodes respectively. Custom made 2 mm path length quartz cuvette (volume: 1.2 mL) was employed for all oxidative spectroelectrochemical measurements. The error within the absorbance maxima is ± 1 nm.

2.4.2.4 Reductive Spectroelectrochemistry

Reductive spectroelectrochemistry (Chapter 3) was carried out in the University of Groningen, under the supervision of Dr. W.R. Browne. UV-Vis data was recorded using an AvaSoft 7.3 software controlled spectrometer (Avantes) with an Avalight balanced deuterium-halogen light source. The potentials were controlled using bulk electrolysis on a model CHI760C potentiostat (CH Instruments, Inc.). Analyte concentrations were typically 0.5-1.0 mM. Anhydrous acetonitrile containing 0.1 M tetrabutylammonium hexafluorophosphate ($TBAPF_6$) was used as the electrolyte. Platinum gauze working electrode, Pt wire counter electrode and a Ag wire reference electrode were employed. Custom made 2 mm path length quartz cuvette was used. The error within the aabsorbance maxima is ± 0.25 nm.

2.4.2.5 Raman Spectroscopy

Excited state resonance Raman spectra (Chapter 3) were obtained with excitation at 400.8 (50 mW at source, PowerTechnology), 449 nm (35 mW at source, PowerTechnology), 473 (100 mW at source, Cobolt Lasers), 532 nm (300 mW at source, Cobolt Lasers), 561 nm (100 mW at source, Cobolt Lasers) and 355 nm (10 Hz 3 mJ per pulse, Spitlight 200, Innolas) to the sample through a 5 cm diameter plano convex lens (f = 6 cm) and Raman scattering collected in a 180^o back-scattering arrangement. Transient Raman spectra were obtained at 355nm with a pulsed laser (10mJ per pulse at sample). The collimated Raman scattering was focused by a second 5 cm diameter plano-convex lens (f = 6 cm) through an appropriate long pass edge filter (Semrock) into a Shamrock300 spectrograph (Andor Technology) with a 1200 l/mm grating blazed at 500 nm and collected by a Newton EMCCD (Andor Technology) operating in conventional ccd mode. Data were recorded and

processed using Solis (Andor Technology) with spectral calibration performed using the Raman spectrum of acetonitrile:toluene 50:50 (v:v). Samples were held in quartz 10 mm pathlength cuvettes. Each compound was dissolved in acetonitrile.

Surface enhanced Raman spectroscopy (SERS) spectra (Chapter 3) were recorded using a Perkin Elmer Raman station with excitation at 735 nm. Each compound was dissolved in water prior to aggregation with Au colloid. The spectra obtained using the Au slides and Au bead were recorded in air.

2.4.2.6 Compounds within This Thesis

The ruthenium and osmium complexes discussed in Chapters 3 and 4 were sourced from within the Prof. J.G. Vos research group and were synthesised by Laura Cleary and Dr. Lynda Cassidy. The work presented in Chapter 5 discusses the electrochemical and spectroelectrochemical properties of an organic tetrathiafulvalene derivative, 5,6 – dehydro-5,6-di(pyrid-4-yl)-bis(ethylenedithio)tetrathiafulvalene (referred to as dipyrBEDT-TTF within this thesis). This work is in collaboration with the Prof. J.D. Wallis research group in Nottingham Trent University, UK, where the compound was synthesised. Finally, the diiron hydrogenase analogues detailed in Chapter 6 are potentially useful as catalysts for hydrogen production. These compounds have been synthesised by our collaborators in the Prof. W. Weigand research group in the University of Jena, Germany.

2.5 Conclusion

This chapter is comprised of an introduction into the theory surrounding the electrode/solution interface and the electrochemical reactions occurring therein. At the electrode/solution interface, polarisation of solvent molecules leads to a build up of charge on the solution side of the interface. The electrode then responds by forming a layer of ions at the surface which is of equal quantity but opposite sign. This is known as the double layer which consists of inner and outer layers known as the Inner Helmholtz Plane (IHP) and Outer Helmholtz Plane (OHP) respectively. The Marcus theory is discussed in section 2.1.4 and is used to describe electron transfer reactions. This theory can be broadly applied to both homogeneous (where no external driving force is required for electron transfer) and heterogeneous electron transfer which encompasses this process occurring at electrode/solution interfaces. Heterogeneous electron transfer may be described as adiabatic or non-adiabatic depending on the extent of coupling between the donor and acceptor units.

Cyclic voltammetry and differential pulse voltammetry are the two principle electrochemical techniques employed throughout this thesis. Cyclic voltammetry is a potential sweep method where the signal is a voltage ramp and the potential is varied linearly with time. Differential pulse voltammetry is an electrochemical technique which optimises the ratio of the Faradaic current to the background capacitive charging current. This ensures heightened sensitivity toward the electrochemical response as the current is measured over a series of steps. This staircase voltammetric method is applied as an accompaniment to cyclic voltammetry in this thesis.

The electronic properties of transition metal complexes are discussed in section 2.2. An introduction into the theory behind absorbance and emission spectroscopy is included in this section as is an introduction into Raman spectroscopy. Finally, the experimental conditions associated with the different techniques used in each chapter are included in section 2.4.

2.6 Bibliography

1 Hibbert, D.B., *Introduction to Electrochemistry*, Macmillan Press Ltd, London, UK, **1993**.

2 Bard, A.J., Faulkner, L.R., *Electrochemical Methods: Fundamentals and Applications*, 2nd Ed., John Wiley & Sons, Inc., USA, **2001**.

3 Forster, R.J., Keyes, T.E., Vos, J.G., *Interfacial Supramolecular Assemblies*, John Wiley & Sons Ltd., Chichester, England, **2003**.

4 Helmholtz, H.L.F., *Ann. Physik*, **1853**, *89*, 211.

5 (a) Gouy, G., *J. Phys. Radium*, **1910**, *9*, 457, (b) Gouy, G., *Compt. Rend.*, **1910**, *149*, 654.

6 Chapman, D.L., *Phil. Mag.*, **1913**, *25*, 475.

7 Stern, O., *Z. Elektrochem.*, **1924**, *30*, 508.

8 Sawyer, D.T., Sobkowiak, A., Roberts Jr., J. L., *Electrochemistry for chemists*, 2nd Ed., John Wiley & Sons Ltd., New York, **1995**.

9 Campagnoli, E., Ph.D. Thesis, Dublin City University, Dublin, Ireland, **2007**.

10 Porter, M.D., Bright, T.B., Allara, D.L., Chidsey C.E.D., *J. Am. Chem. Soc.*, **1987**, *109*, 3559.

11 Forster, R.J., Faulkner, L.R., *J. Am. Chem. Soc*, **1994**, *116*, 5444.

12 Marcus, R.A., *Angew. Chem., Int. Ed. Engl.*, **1993**, *32*, 1111.

13 Balzani, V., Juris, A., Venturi, M., *Chem. Rev.*, **1996**, *96*, 759.

14 Hage, R., Ph.D. Thesis, Leidin University, The Netherlands, **1991**.

15 Juris, A., Balzani, V., Barigelletti, F., Campagna, S., Belser, P., Von Zelewsky, A., *Coord. Chem. Rev.*, **1988**, *84*, 85.

16 Roffia, S., Casadei, R., Paolucci, F., Paradisi, C., Bignozzi, C.A., Scandola, F., *J. Electroanal. Chem.*, **1991**, *302*, 157.

17 Weiner, M.A., Basu, A., *Inorg. Chem.*, **1980**, *19*, 2797.

18 Pinnick, D.V., Durham, B., *Inorg. Chem.*, **1984**, *23*, 1440.

19 (a) Franck, J., *Trans. Far. Soc.*, **1926**, *21*, 536, (b) Condon, E., *Phys. Rev.*, **1926**, *27*, 640, (c) Condon, E., *Phys. Rev.*, **1926**, *28*, 1182, (d) Condon, E., *Phys. Rev.*, **1928**, *32*, 858.

20 Hurenkamp, J.H., Ph.D. Thesis, University of Groningen, The Netherlands, **2008**.

21 Kasha, M, *Disscus. Faraday Soc.*, **1950**, *9*, 14.

22 Seddon, E.A., Seddon, K.R., *The Chemistry of Ruthenium*, Elsevier, Amsterdam, **1984**.

23 Lytle, F.E., Hercules, D.M., *J. Am. Chem. Soc.*, **1969**, *91*, 253.

24 Klassen, D.M., Crosby, G.A., *J. Chem. Phys.*, **1968**, *48*, 1853.

25 Paris, J.P., Brandt, W.W., *J. Am. Chem. Soc.*, **1959**, *81*, 5001.

26 Demas, J.A., Crosby, G.A., *J. Mol. Spectrosc.*, **1968**, *26*, 72.

27 Browne, W.R., O'Boyle, N.M., McGarvey, J.J., Vos, J.G., *Chem. Soc. Rev.*, **2005**, *34*, 641.

28 Keyes, T.E., Forster, R.J., *Handbook of Electrochemistry*, Ed C.G. Zoski, Elsevier Science, **2007**.

29 Browne, W.R., O'Boyle, N.M., McGarvey, J.J., Vos, J.G., *Chem. Soc. Rev.*, **2005**, *34*, 641.

30 Albrecht, M.G., Creighton, J.A., *J. Am. Chem. Soc.*, **1977**, *99*, 5215.

31 Trasatti, S., Petrii, O.A., *J. Electroanal. Chem.*, **1992**, *327*, 353.